Ultrasound in Med. & Biol., Vol. 39, No. 11, pp. 2053–2065, 2013

0301-5629/$ - see front matter

http://dx.doi.org/10.1016/j.ultrasmedbio.2013.04.022

● *Original Contribution*

EVALUATION OF BI-VENTRICULAR CORONARY FLOW PATTERNS USING HIGH-FREQUENCY ULTRASOUND IN MICE WITH TRANSVERSE AORTIC CONSTRICTION

JIAN WU,*†‡ YU-QING ZHOU,* YUNZENG ZOU,†‡ and MARK HENKELMAN*§

*Mouse Imaging Centre, The Hospital for Sick Children, Toronto, Canada; †Shanghai Institute of Cardiovascular Diseases, Zhongshan Hospital, Shanghai, China; ‡Institutes of Biomedical Sciences, Fudan University, Shanghai, China; and §Department of Medical Biophysics, University of Toronto, Toronto, Canada

(*Received* 13 *November* 2012; *revised* 15 *March* 2013; *in final form* 28 *April* 2013)

Abstract—Using high-frequency color and pulsed Doppler ultrasound, we evaluated the flow patterns of the left (LCA), septal (SCA) and right (RCA) coronary arteries in mice with and without transverse aortic constriction (TAC). Fifty-two male C57BL/6J mice were subjected to TAC or a corresponding sham operation. At 2 and 8 wk post-surgery, Doppler flow spectra from the three coronary arteries, together with morphologic and functional parameters of the left and right ventricles, were measured. Histology was performed to evaluate myocyte size and neo-angiogenesis in both ventricles. In sham-operated mice, the LCA and SCA both exhibited low-flow waveforms during systole and dominantly higher-flow waveforms during diastole. The RCA exhibited generally lower flow velocity, with similar systolic and diastolic waveforms. TAC significantly increased the systolic flow velocities of all coronary arteries, but enhanced the flow mainly in the LCA and SCA. In the left ventricle, coronary flow reserve was partially preserved 2 wk post-TAC, but decreased at 8 wk, consistent with changes in neo-angiogenesis and systolic function. In contrast, no significant change was found in the coronary flow reserve, structure or function of the right ventricle. This study has established a protocol for evaluating the flow pattern in three principal coronary arteries in mice using Doppler ultrasound and illustrated the difference among three vessels at baseline. In mice with TAC, the difference in the associating pattern of coronary flow dynamics with the myocardial structure and function between the left and right ventricles provides further insights into ventricular remodeling under pressure overload. (E-mail: yqzhou@mouseimaging.ca) © **2013 World Federation for Ultrasound in Medicine & Biology.**

Key Words: **Mice, Coronary artery, Flow dynamics, Doppler, Transverse aortic constriction.**

INTRODUCTION

Genetically engineered mice are now the most popular model systems for identifying genetic causes and designing effective therapeutics for human cardiovascular diseases (Yutzey and Robbins 2007). Numerous mouse strains have become available for studying coronary arterial diseases such as atherosclerosis and myocardial ischemia (Braun et al. 2002; Li et al. 2001). As a consequence, phenotyping of the mouse cardiovascular system using non-invasive micro-imaging technologies is in ever-increasing demand, but still faces challenges (Hartley et al. 2002; Tobita et al. 2010), especially for the *in vivo* observation of small but vital vasculature such as the coronary arteries.

High-frequency (30–45 MHz) ultrasound systems dedicated to small animal imaging became available a decade ago and have been widely used for cardiac structural, functional and hemodynamic evaluation of mice (Zhou et al. 2004). A few groups have attempted Doppler ultrasound to estimate coronary flow dynamics, but limited to the left coronary artery (LCA) (Hartley et al. 2008; Saraste et al. 2008; Wikström et al. 2005). Only with the recent advent of Doppler color flow imaging (Foster et al. 2009) has it become possible to visualize the right coronary artery (RCA) and the septal coronary artery (SCA), which are smaller and anatomically more variable than the LCA (Fernandez et al. 2008; Icardo and Colvee 2001). To the best of our knowledge, no data are available related to the flow dynamics of the RCA and SCA, nor has there been any comparison of

Address correspondence to: Yu-Qing Zhou, The Hospital for Sick Children, Mouse Imaging Centre, 25 Orde Street, Toronto, ON, Canada M5T 3H7. E-mail: yqzhou@mouseimaging.ca

the coronary flow dynamics between the left and right sides of the heart in mice.

Physiologic perturbations by surgical interventions such as transversal aortic constriction (TAC) and coronary arterial ligation can facilitate the in-depth exploration into the underlying mechanisms of specific disease conditions including pressure overload and myocardial ischemia (Tarnavski et al. 2004). The mouse with TAC has been used to induce pressure overload to the left ventricle for observation and intervention of the ventricular remodeling (Rockman et al. 1991). The flow dynamics of all coronary arteries at different stages after TAC would provide valuable insights into this disease process. TAC results in similarly elevated perfusion pressure (from the aorta) to all coronary arteries, but different loading conditions to the left and right ventricles. The left ventricle faces significantly elevated aortic pressure during systole, whereas the right ventricle experiences little change in pressure load from the pulmonary artery (Ito et al. 1994). Therefore, it is of considerable interest to compare the flow dynamics of the LCA and SCA with that of RCA for differentiating the effects of the altered perfusion pressure to all coronary arteries and the pressure overload to the left ventricle.

This study was conducted to establish a protocol for imaging all three principal coronary arteries in mice using high-frequency Doppler ultrasound for the first time and to evaluate the flow dynamics of these coronary arteries at baseline. Then, in mice with TAC, the flow dynamics of the three coronary arteries was evaluated in the early hypertrophic stage with compensated cardiac function and in the late transitional stage to heart failure. All coronary Doppler flow parameters were associated with corresponding structural and functional changes of the left and right ventricles.

METHODS

Animals

The experimental protocol of this study was approved by the Institutional Animal Care and Use Committee of the Hospital for Sick Children, Toronto. A total of 52 male C57BL/6J mice 12–13 wk of age (The Jackson Laboratory, Bar Harbor, ME, USA) were divided into four groups. Two groups were subjected to surgically induced TAC, and the other two groups had sham surgery and served as controls. At each of two time points of observation, 2 wk (functionally compensatory stage) and 8 wk (transitional stage to heart failure) post-surgery (Ceci et al. 2007; Sano et al. 2007), one group of mice with TAC and one sham-operated group underwent ultrasound imaging and were immediately sacrificed for histology. Mice were housed in an air-conditioned room with a 12:12-h light:dark cycle and received standard mouse chow and water *ad libitum*.

Surgery

Transverse aortic constriction was created as described previously (Wu et al. 2012b). Briefly, mice were anesthetized by intraperitoneal injection of a mixture of ketamine (150 mg/kg) and xylazine (10 mg/kg), endotracheally intubated and cannulated to a rodent ventilator. The chest was opened and the aortic arch was exposed. The aorta was constricted between the innominate artery and the left common carotid artery with 6-O silk suture by ligating the aorta against a 26-gauge blunted needle, which was withdrawn immediately after ligation. The chest was then closed, and air in the chest was expelled. Meloxicam (0.13 mg/mouse) was given to reduce pain. Mice were placed on heating pads until awake and then returned to their cages.

Ultrasound imaging

A Vevo 2100 ultrasound system (VisualSonics, Toronto, ON, Canada) with a 30-MHz linear array transducer was used. The image resolution was $\sim$110 μm (laterally) by $\sim$50 μm (axially). With proper settings (low pulse repetition frequency $<$12.5 kHz, appropriate gain and wall filter levels), Doppler color flow imaging clearly visualized mouse coronary arteries and guided the pulsed wave Doppler flow recording. The pulsed Doppler sample volume had a lateral dimension of 150 μm, and its axial dimension was adjusted between 100 and 200 μm according to the size of the targeted vessel. During ultrasound imaging, animals were anesthetized using isoflurane at 1.5% by face mask (Zhou et al. 2004).

Estimation of TAC severity

Transverse aortic constriction of different degrees results in a variable left ventricular end-systolic pressure and ventricular hypertrophy (Li et al. 2003). As previously reported by others (Bjørnstad et al. 2011) and ourselves (Wu et al. 2012b), the Doppler jet flow velocity at the constriction site and the peak velocity ratio between the right and left common carotid arteries were able to reflect the left ventricular end-systolic pressure, and mice with a jet flow velocity$<$3 m/s and ratio $<$3 failed to produce adequate left ventricular hypertrophy. According to these criteria, three mice were dropped in this study after the measurement 2 wk post-TAC.

Morphologic and functional measurements of left and right ventricles

The dimensions and the systolic and diastolic functions of both ventricles were measured *in vivo* as described previously (Zhou et al. 2004, 2005). Under

the guidance of 2-D ultrasound imaging, the left ventricular anterior and posterior wall thicknesses and chamber dimensions were measured using M-mode recording, and the left ventricular fractional shortening and ejection fraction were calculated. In an oblique section from the left para-sternal imaging window showing the right side of the heart in the far field of the image (Zhou et al. 2004) (Fig. 1a), the right ventricular free wall thickness was also measured using M-mode. The Doppler spectra in the mitral and tricuspid orifices were recorded from apical four-chamber views to evaluate the diastolic function of the left and right ventricles.

Coronary flow recording in baseline condition

In mice, the LCA is the largest coronary artery with a relatively consistent origin and branching, irrigating most of left ventricle except for the septum (Ahn et al. 2004). Differing from humans, where the interventriclar septum is supplied by small branches from the LCA and the RCA (James and Burch 1958), mice have a dedicated vessel, the SCA, supplying blood to the septum. The SCA originates from the RCA or right aortic sinus (34%), LCA or sinus (26%) or both (40%) (Fernandez et al. 2008), and mostly runs along the right side of the ventricular septum.

The LCA was imaged from a left para-sternal long-axis view, with the imaging section at ~45° to the coronal plane of the mouse body. In this view, the left ventricular outflow tract, aortic orifice and ascending aorta were visualized in the middle field of the image (Zhou et al. 2004). In Doppler color flow imaging, the LCA presented as a red stripe originating from the aortic sinus and running along the surface of the left ventricular wall. With the pulsed Doppler sample volume placed ~2 mm distal to its origin, the flow spectrum with a small systolic waveform and a dominantly higher diastolic waveform was recorded (Fig. 1a).

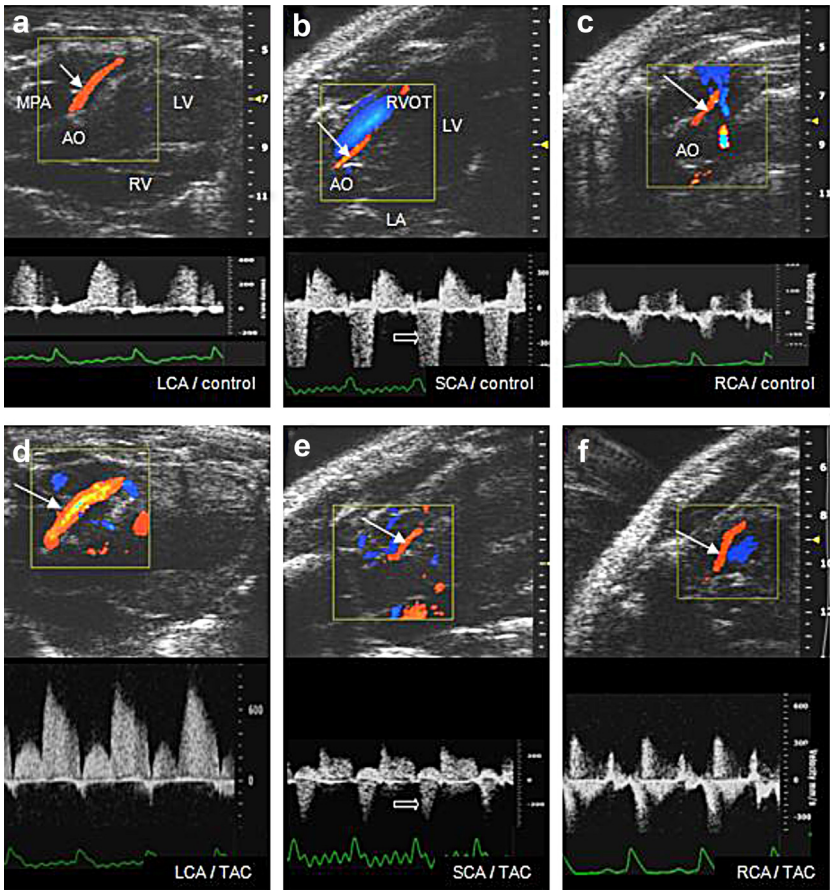

Fig. 1. Representative Doppler color flow images and pulsed wave Doppler flow velocity recordings of coronary arteries 2 wk after transverse aortic constriction (TAC) or sham surgery. (a–c) Recordings from the left (LCA), septal (SCA) and right (RCA) coronary arteries of sham-operated mice, respectively. (d–f) Recordings from the LCA, SCA and RCA of mice with TAC, respectively. *White solid arrows* indicate the locations of pulsed Doppler sample volume for velocity recording. *Open arrows* indicate the systolic outflow recorded from the right ventricular outflow tract (RVOT). AO = aortic orifice, LA = left atrium, LV = left ventricle, RV = right ventricle.

The SCA was imaged from a right para-sternal window, with the transducer located at the lower half of the chest and pointed posteriorly and upward. The imaging section was initially parallel to the central axis of the mouse body, but slightly tilted to the left. Further fine adjustment was made until the left and right ventricular outflow tracts, as well as the inter-ventricular septum between them, were visualized in their longitudinal axes. The SCA presented as a red stripe along the right surface of the ventricular septum in Doppler color flow imaging, and its pulsed Doppler flow spectrum recorded ~1 mm distal to its origin was characterized by a very small and positive systolic waveform followed by a large and positive diastolic waveform. We measured the flow from the main stem of the SCA along the right side of the septum, but did not intend to distinguish where the SCA originated from. There often was a negative waveform with higher amplitude during systole, which was the systolic outflow in the adjacent right ventricular outflow tract (Fig. 1b).

For the RCA, the transducer was rotated clockwise by 30–45° from the previous position for the SCA, until the right ventricular outflow tract and septum totally disappeared from the image. In this view, the aortic root in an oblique section was visualized, with the RCA presenting as a red stripe originating from the right aortic sinus. Its pulsed Doppler spectrum recorded ~1 mm distal to its origin was characterized by the generally low velocity (relative to those of the LCA and the SCA) and the similar peak velocities of the systolic and diastolic waveforms, with their division hard to identify (Fig. 1c). The RCA had relatively large movement with the right ventricular wall, and therefore, a larger pulsed Doppler sample volume was applied to cover the targeted vessel for flow recording. Consequently, the flow signals from the adjacent vessels made the RCA Doppler flow spectrum less clean (with negative waveforms from coronary veins) than those from the LCA and SCA.

Coronary flow recording in hyperemia induced by adenosine

After the baseline flow recording, adenosine (Astellas Pharma, Markham, ON, Canada) was infused intravenously *via* the tail vein with an infusion pump at the rate of 160 μg/kg/min to induce hyperemia (Wikström et al. 2005), and Doppler flow spectra were again recorded for each of the three coronary arteries (Fig. 1d–f) after ~3 min of infusion, when the heart rate and respiration became stable.

In Doppler flow recording, significant effort was made to reduce the intercept angle between Doppler beam and flow direction. In no recording did the angle exceed 60°. The electrocardiogram (ECG) was simultaneously recorded to identify the systolic and diastolic flow waveforms. For the LCA and SCA, the systolic and diastolic waveforms had clear division, and the peak velocity and mean velocity of individual waveforms were measured by tracing the maximal contour of the Doppler spectrum. For the RCA, separation of the systolic and diastolic waveforms was often difficult, and therefore the peak velocities of the two waveforms and the mean velocity of the whole flow spectrum throughout cardiac cycle were measured. For the LCA and SCA, coronary flow reserve (CFR) was calculated in two ways: (i) the ratio of the mean velocity of the diastolic waveform (MV_D) during hyperemia to the corresponding value at baseline; (ii) the ratio of the mean velocity of both systolic and diastolic waveforms (MV_{S+D}) during hyperemia to the corresponding value at baseline. In the TAC model, the elevated aortic pressure significantly increases coronary flow during systole and may consequently reduce the room for further dilation of the coronary arteries during diastole when a vasodilator is used. Therefore, the systolic waveform was also included in measuring CFR. For the RCA, only the ratio of the mean velocity of both systolic and diastolic waveforms (MV_{S+D}) during hyperemia to the corresponding value at baseline was calculated as CFR.

Histology

After ultrasound imaging at each time point of observation, mice with TAC and sham-operated mice were euthanized, and the hearts were excised. The atria were removed, and the ventricles weighed and fixed in 4% paraformaldehyde, washed in phosphate-buffered saline and then dehydrated in 70% ethanol. The ventricles were embedded in paraffin and sectioned at 5 μm in the short axis at the mid-ventricular level. To observe myocytes, slides were stained with Nova Red through the specific combination of biotin-conjugated wheat germ agglutinin (L5142, Sigma, St Louis, MO, USA) with myocyte membrane. To count capillaries, additional slides were stained with Nova Red through the targeted binding of rabbit polyclonal anti-CD31 antibody (ab28364, AbCam, Cambridge, UK) to endothelium. The slides were scanned with a digital scanner (DSM 3.1, Trestle, Newport Beach, CA, USA) and measurements were made off-line in the left ventricular lateral wall, septum and right ventricular free wall at 10 × 40 magnification. The myocyte size in each ventricular wall was measured in 20 randomly selected myocytes with round shape and nucleus, and calculated as the average of two perpendicular diameter measurements. For capillary density, CD31-positive vessels (brown) and myocytes (light blue) were counted within the same region, and the number of capillaries per myocyte was calculated.

Statistics

All measured parameters are expressed as the mean ± standard error of the mean. All statistical evaluations were performed with SPSS Version 15.0 software (SPSS Inc., Chicago, IL, USA). Differences between the TAC and corresponding sham-operated groups or between the different time points of observation were evaluated with an unpaired Student's *t*-test. The data from three coronary arteries in the TAC and corresponding sham-operated groups were analyzed using two-way analysis of variance with *post hoc* analysis by a Student-Newman-Keuls correction. Values of $p < 0.05$ were considered statistically significant.

RESULTS

Of 52 mice, 4 died during surgery and 6 died after surgery before the final ultrasound imaging. Three mice with insufficient TAC did not meet the criteria for further study. Thirty-nine mice were included in the data analysis. Tail vein cannulation failed in 2 mice, with loss of hyperemia measurements. At baseline, the LCA was mostly accessible, with the success rate of pulsed Doppler flow recording at 97%. The SCA and RCA were measured at success rates of 87% and 92%, respectively. In mice with TAC, all coronary arteries were easier to visualize probably because of the dilation of the lumen and increase in flow velocity.

Table 1. General information, left and right ventricular dimensions and systolic and diastolic functions in all sham-operated mice and mice with TAC 2 and 8 wk post-surgery

	2 wk		8 wk	
Parameter	Sham	TAC	Sham	TAC
Number of mice	8	10	9	12
Body weight (BW) (g)	30.7 ± 0.9	30.3 ± 0.7	34.1 ± 0.7†	30.9 ± 1.0*
Heart weight (HW) (mg)	122.6 ± 4.1	155.1 ± 6.9*	130.1 ± 1.8	191.0 ± 14.8*†
HW/BW (mg/g)	4.00 ± 0.10	5.07 ± 0.23*	3.82 ± 0.06	6.29 ± 0.59*
V_{max} at banding site (m/s)	1.05 ± 0.05	3.74 ± 0.12*	0.90 ± 0.06	3.72 ± 0.14*
RCCA-PV/LCCA-PV	1.17 ± 0.13	6.93 ± 1.27*	1.10 ± 0.06*	5.39 ± 0.55
Left ventricular dimensions and systolic function by M-mode				
Number of mice	8	9	9	11
AW_s (mm)	1.22 ± 0.04	1.46 ± 0.05*	1.24 ± 0.04	1.49 ± 0.04*
ESD (mm)	2.87 ± 0.11	2.84 ± 0.13	2.87 ± 0.10	3.32 ± 0.20
PW_s (mm)	1.10 ± 0.03	1.32 ± 0.08*	1.10 ± 0.04	1.32 ± 0.05*
AW_d (mm)	0.84 ± 0.04	1.07 ± 0.04*	0.88 ± 0.03	1.12 ± 0.05*
EDD (mm)	3.98 ± 0.12	4.01 ± 0.13	3.97 ± 0.08	4.23 ± 0.17
PW_d (mm)	0.84 ± 0.04	0.99 ± 0.05*	0.81 ± 0.03	1.06 ± 0.04*
EF (%)	54.4 ± 1.8	56.7 ± 2.5	54.4 ± 2.1	44.5 ± 3.4*†
FS (%)	27.8 ± 1.2	29.5 ± 1.6	27.9 ± 1.4	22.1 ± 1.9*†
Mitral inflow by Doppler				
Number of mice	8	10	9	9
Heart rate (bpm)	429 ± 20	458 ± 17	399 ± 20	443 ± 18
Peak E (cm/s)	67.5 ± 2.0	70.8 ± 2.2	62.6 ± 2.4	67.2 ± 4.1
Peak A (cm/s)	48.6 ± 2.8	59.5 ± 3.5*	46.6 ± 2.0	62.2 ± 5.6*
E/A	1.42 ± 0.07	1.22 ± 0.06*	1.36 ± 0.06	1.12 ± 0.07*
Right ventricular wall thickness by M-mode				
Number of mice	8	10	9	11
FWs (mm)	0.51 ± 0.05	0.55 ± 0.05	0.52 ± 0.02	0.58 ± 0.03
FWd (mm)	0.38 ± 0.06	0.35 ± 0.03	0.35 ± 0.01	0.38 ± 0.02
Tricuspid inflow by Doppler				
Number of mice	7	9	7	6
Heart rate (bpm)	425 ± 13	447 ± 15	395 ± 12	415 ± 18
Peak E (cm/s)	28.9 ± 2.4	28.3 ± 1.3	25.5 ± 1.8	26.6 ± 5.5
Peak A (cm/s)	54.6 ± 3.4	52.2 ± 1.5	46.9 ± 2.5	52.9 ± 6.3
E/A	0.53 ± 0.02	0.54 ± 0.02	0.54 ± 0.02	0.49 ± 0.06

TAC = transverse aortic constriction; RCCA-PV/LCCA-PV = ratio of peak velocity of right common carotid artery to that of left common carotid artery; V_{max} = maximal velocity at site of TAC; AW_d (AW_s) = anterior wall end-diastolic (end-systolic) thickness of left ventricle; EDD (ESD) = end-diastolic (end-systolic) chamber dimensions of left ventricle; PW_d (PW_s) = posterior wall end-diastolic (end-systolic) thickness of left ventricle; EF = ejection fraction of left ventricle; FS = fractional shortening of left ventricle; peak E = peak of early diastolic inflow velocity caused by ventricular active relaxation in either mitral or tricuspid inflow Doppler velocity recordings; peak A = peak of late diastolic inflow velocity caused by atrial contraction in either mitral or tricuspid inflow Doppler velocity recordings; E/A = ratio of peak E velocity to peak A velocity; FW_d (FW_s) = free wall end-diastolic (end-systolic) thickness of right ventricle.

Results are expressed as the mean ± standard error of the mean.

* $p < 0.05$ versus corresponding value of sham control group at the same time point of observation.

† $p < 0.05$ versus value of corresponding group 2 wk post-surgery.

Changes in the dimensions and functions of left and right ventricles caused by TAC

Compared with sham-operated mice, mice with TAC had a significant increase in left ventricular wall thickness and a deterioration in left ventricular diastolic function (represented by the peak E/A ratio of mitral inflow) at both time points of observation, but a decrease in left ventricular systolic function only at 8 wk post-TAC (6 of 11 mice had fractional shortening <25% and an ejection fraction <50%). In contrast, right ventricular wall thickness was normal post-surgery. Right ventricular diastolic function (determined by the peak E/A ratio of the tricuspid inflow) remained unchanged at both time points (Table 1).

Difference in flow patterns among three coronary arteries at baseline

As seen in Table 2, flow patterns significantly differed between the three coronary arteries at baseline. The flow spectra of both the LCA and SCA had smaller systolic waveforms and much larger diastolic waveforms, with clear division between the two waveforms. The RCA spectrum had similar peak velocities between systolic and diastolic waveforms, which did not exhibit a clear division. Generally, the LCA flow velocity was the highest, the SCA intermediate, and the RCA the lowest (Table 2 and Figs. 2–4).

Change in coronary flow pattern caused by TAC

For the LCA, overall mean flow velocity increased in mice with TAC mice, compared with that in sham-operated mice, because of the significant increase in both systolic and diastolic flow components at both time points of observation, both at baseline and during hyperemia. Two weeks post-TAC, the CFR calculated using the mean velocity of the diastolic waveform (MV_D) significantly differed between the two groups, but the CFR calculated using the overall mean velocity of both systolic and diastolic waveforms (MV_{S+D}) did not. At 8 wk, the CFRs calculated in both ways significantly decreased in mice with TAC compared with those in controls (Figs. 1a, d and 2).

For the SCA, flow velocity also increased in mice with TAC compared with sham-operated mice, in a similar way as for the LCA, but significantly only at 8 wk post surgery. The CFRs in mice with TAC were completely normal at 2 wk, but significantly decreased at 8 wk post-surgery (Figs. 1b, e and 3).

For the RCA, peak systolic velocity increased significantly, but overall mean velocity did not significantly change in mice with TAC at any time point of observation. Unlike the LCA and SCA, the CFR of the RCA did not exhibit any significant change during the entire course of observation (Figs. 1c, f and 4).

After the infusion of adenosine, heart rate tended to increase slightly compared with that at baseline, but did

Table 2. Comparison of Doppler flow parameters of three coronary arteries in sham-operated mice and mice with TAC 2 wk post-surgery

Parameter	Left coronary artery	Septal coronary artery	Right coronary artery
Sham-operated group (n = 8)			
Heart rate (bpm)	465 ± 13	469 ± 15	460 ± 15
PSV (cm/s)	10.3 ± 1.4	6.5 ± 0.8†	14.6 ± 0.9†,‡
PDV (cm/s)	41.8 ± 2.3	29.3 ± 2.5†	18.7 ± 0.9†,‡
PSV/PDV	0.26 ± 0.04	0.22 ± 0.01	0.78 ± 0.04†,‡
MV_S (cm/s)	7.2 ± 1.1	5.5 ± 0.6	—
MV_D (cm/s)	27.1 ± 0.9	18.5 ± 1.4†	—
MV_S/MV_D	0.27 ± 0.04	0.29 ± 0.01	—
MV_{S+D} (cm/s)	22.0 ± 0.8	14.1 ± 1.0†	9.8 ± 1.2†,‡
TAC group (n = 10)			
Heart rate (bpm)	505 ± 16	471 ± 17	486 ± 19
PSV (cm/s)	29.8 ± 6.7*	16.1 ± 4.6	27.6 ± 4.1*
PDV (cm/s)	67.5 ± 7.7*	33.7 ± 4.7†	25.6 ± 3.9†
PSV/PDV	0.41 ± 0.05*	0.47 ± 0.12	1.10 ± 0.06*,†,‡
MV_S (cm/s)	26.9 ± 7.3*	11.8 ± 3.1	—
MV_D (cm/s)	48.2 ± 5.8*	22.9 ± 2.9†	—
MV_S/MV_D	0.50 ± 0.08*	0.52 ± 0.12	—
MV_{S+D} (cm/s)	39.7 ± 5.8*	18.4 ± 2.4†	13.4 ± 2.7†

TAC = transverse aortic constriction; MV_D = mean velocity of diastolic waveform; MV_S = mean velocity of systolic waveform; MV_{S+D} = mean velocity of both systolic and diastolic waveforms throughout the cardiac cycle; PDV = peak diastolic velocity; PSV = peak systolic velocity.

Differences in MV_S, MV_D and MV_S/MV_D between the left and septal coronary arteries were evaluated with an unpaired Student *t*-test, whereas differences in other indexes between the three coronary arteries were analyzed using a one-way analysis of variance with *post hoc* analysis by Student-Newman-Keuls correction.

* $p < 0.05$ versus corresponding value of sham-operated mice.

† $p < 0.05$ versus corresponding value of left coronary artery.

‡ $p < 0.05$ versus corresponding value of septal coronary artery.

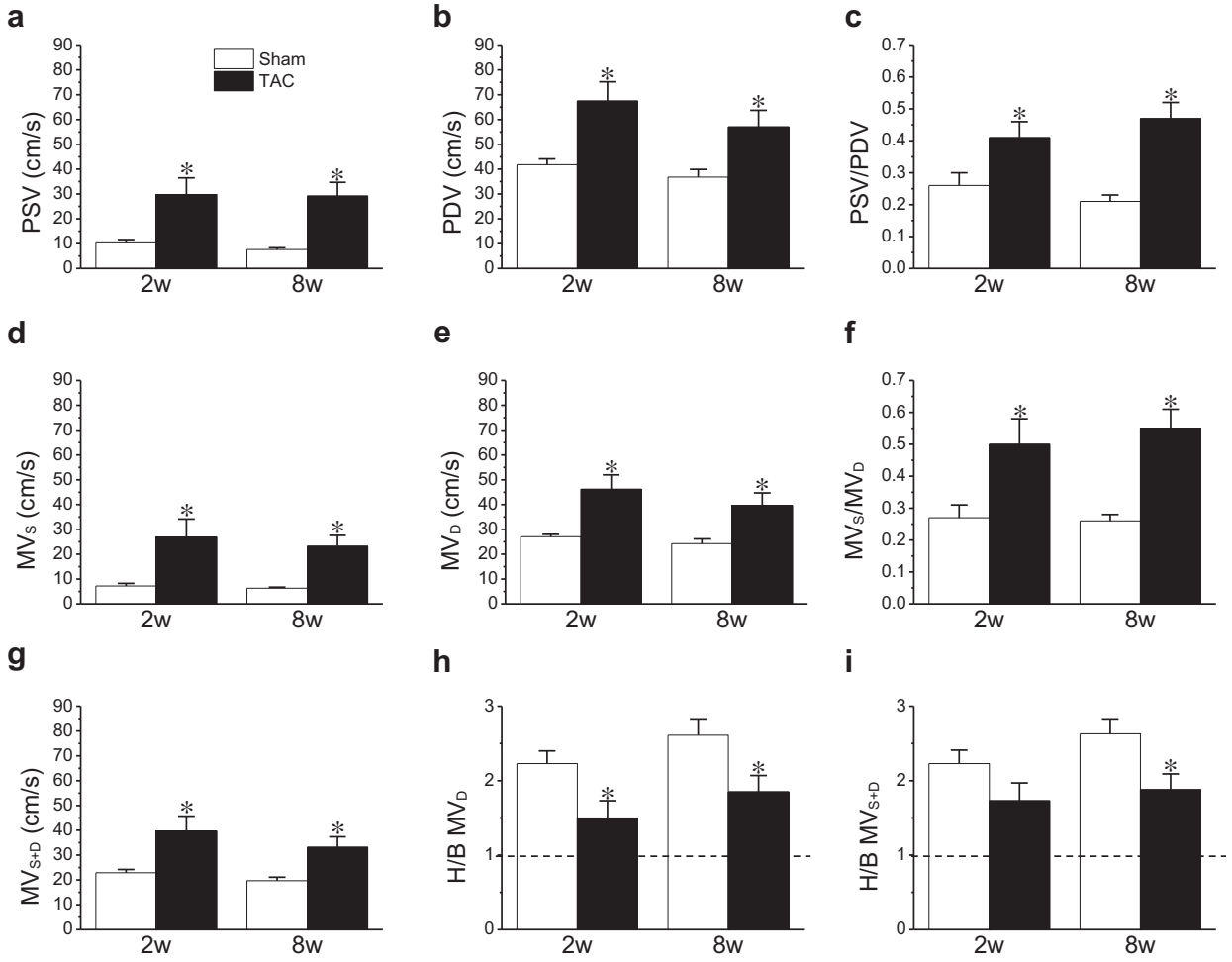

Fig. 2. Baseline Doppler flow parameters (a–g) and coronary flow reserve (CFR) (h, i) measured from the left coronary artery (LCA), with comparison between sham-operated mice and those with transverse aortic constriction (TAC) 2 and 8 wk post-surgery. (a) Peak velocity of systolic wave (PSV). (b) Peak velocity of diastolic wave (PDV). (c) Ratio of PSV to PDV. (d) Mean velocity of systolic wave (MV_S). (e) Mean velocity of diastolic wave (MV_D). (f) Ratio of MV_S to MV_D. (g) Mean velocity of both systolic and diastolic waves throughout the cardiac cycle (MV_{S+D}). (h) Ratio of MV_D in hyperemia induced by venous administration of adenosine to that at baseline (H/B MV_D). (i) Ratio of MV_{S+D} in hyperemia to that at baseline (H/B MV_{S+D}). *$p < 0.05$ versus corresponding value of sham-operated mice.

not differ significantly for any of three coronary arteries in any group of mice at any time point of observation.

Histologic change in ventricular myocardium caused by TAC

Compared with sham-operated mice, mice with TAC had significant increases in wall thickness and myocyte size in the left ventricular lateral wall and septum at both time points of observation, but not in the right ventricular free wall at any time (Figs. 5a–d and 6a–f). On the other hand, mice with TAC had a significant increase in capillary density in the left ventricular lateral wall and septum at 2 wk and a drop back to the level of sham-operated mice at 8 wk post-TAC. For the right ventricular free wall, capillary density was found to be unchanged at either 2 or 8 wk post-surgery (Figs. 5e–h and 6g–i).

DISCUSSION

With the use of high-frequency ultrasound, this study has for the first time established a protocol for quantitatively evaluating the flow dynamics in the three principal coronary arteries in mice, and found significant differences in flow pattern among these vessels. Changes in coronary flow pattern at different stages after TAC also were observed and correlated with ventricular structure and function, with the comparison between the left and right sides of the heart.

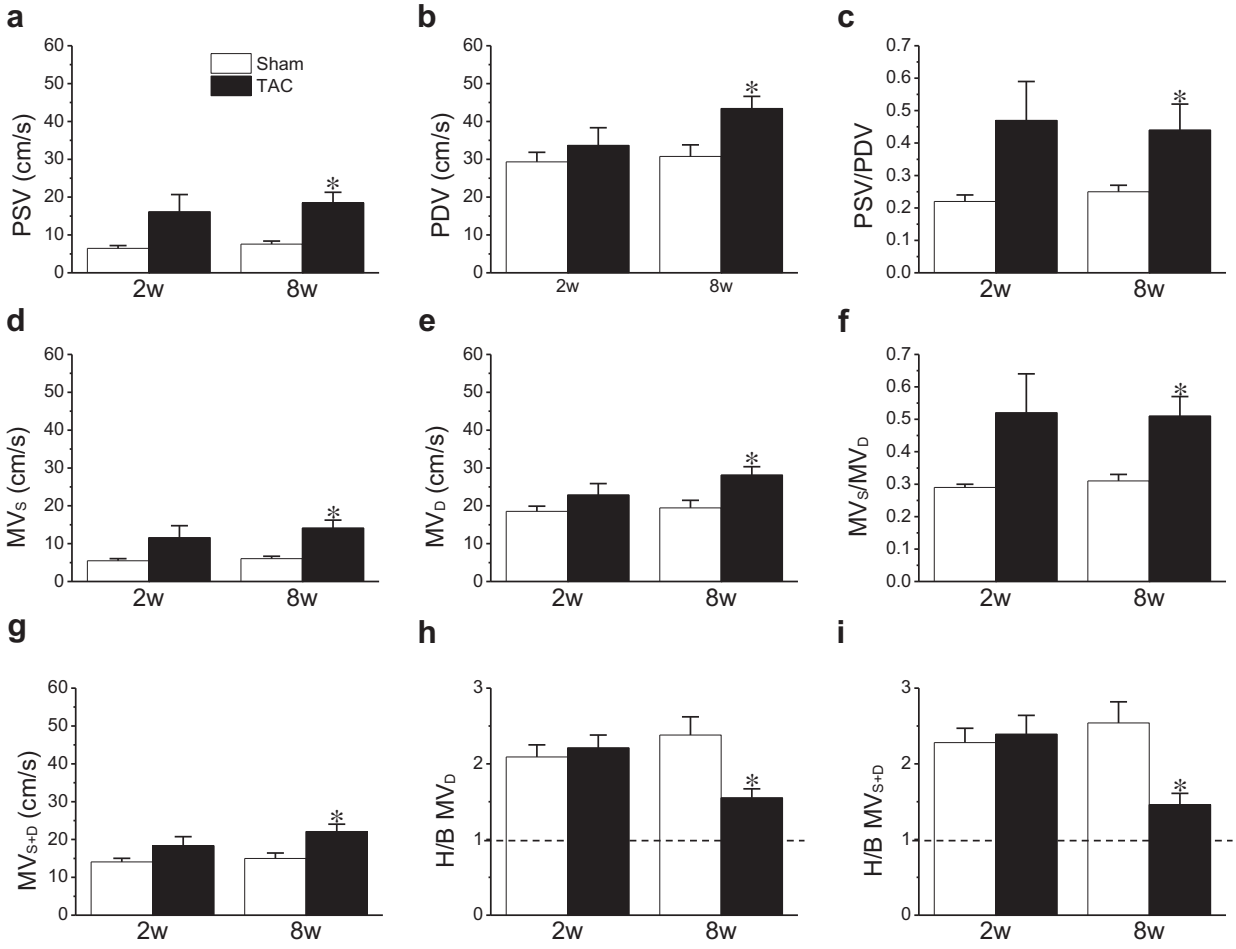

Fig. 3. Baseline Doppler flow parameters (a–g) and coronary flow reserve (CFR) (h, i) measured from the septal coronary artery (SCA), with comparison between sham-operated mice and mice with transverse aortic constriction (TAC) 2 and 8 wk post-surgery. PSV = peak velocity of systolic wave, PDV = peak velocity of diastolic wave, MV_S = mean velocity of systolic wave, MV_D = mean velocity of diastolic wave, MV_{S+D} = mean velocity of both the systolic and diastolic waves throughout the cardiac cycle, H/B MV_D = ratio of MV_D in hyperemia induced by venous administration of adenosine to that at baseline, H/B MV_{S+D} = ratio of MV_{S+D} in hyperemia to that at baseline. *$p < 0.05$ versus corresponding value of sham-operated mice.

Imaging three coronary arteries in mice using ultrasound

Both clinical and high-frequency ultrasound systems have been used to measure coronary flow in mice, but limited to the LCA (Gan et al. 2004; Hartley et al. 2008). The advent of high-frequency Doppler color flow imaging (Foster et al. 2009) makes it possible to visualize the SCA and RCA with relatively low blood flow, even when the lumen of the small vessel is not optimally visualized in the 2-D tissue image. At low pulsed repetition frequency and with a proper wall filter and Doppler gain levels, it is possible to follow all principal coronary arteries to their middle segments and even beyond. Such capability enables quantitative evaluation of the myocardial blood perfusion and the association between flow pattern and atherosclerotic formation in various mouse models.

Normal flow patterns in three coronary arteries

The present study found different phasic flow patterns in three coronary arteries in mice. The LCA flow pattern is characterized by a smaller systolic waveform and a predominantly higher diastolic waveform. As the left ventricle is anatomically dominant compared with the right ventricle (Zhou et al. 2003) and mostly irrigated by the LCA (Ahn et al. 2004; Icardo and Colvee 2001), the LCA has the highest flow velocity compared with the other coronary arteries, but with a large difference between the systolic and diastolic waveforms.

As found in humans, the interaction of aortic pressure, coronary vasculature and myocardial mechanics yields complicated waves driving the blood flow in coronary arteries (Davies et al. 2006; Hadjiloizou et al. 2008). The differences in flow pattern among the various coronary arteries relate to the perfusion bed of

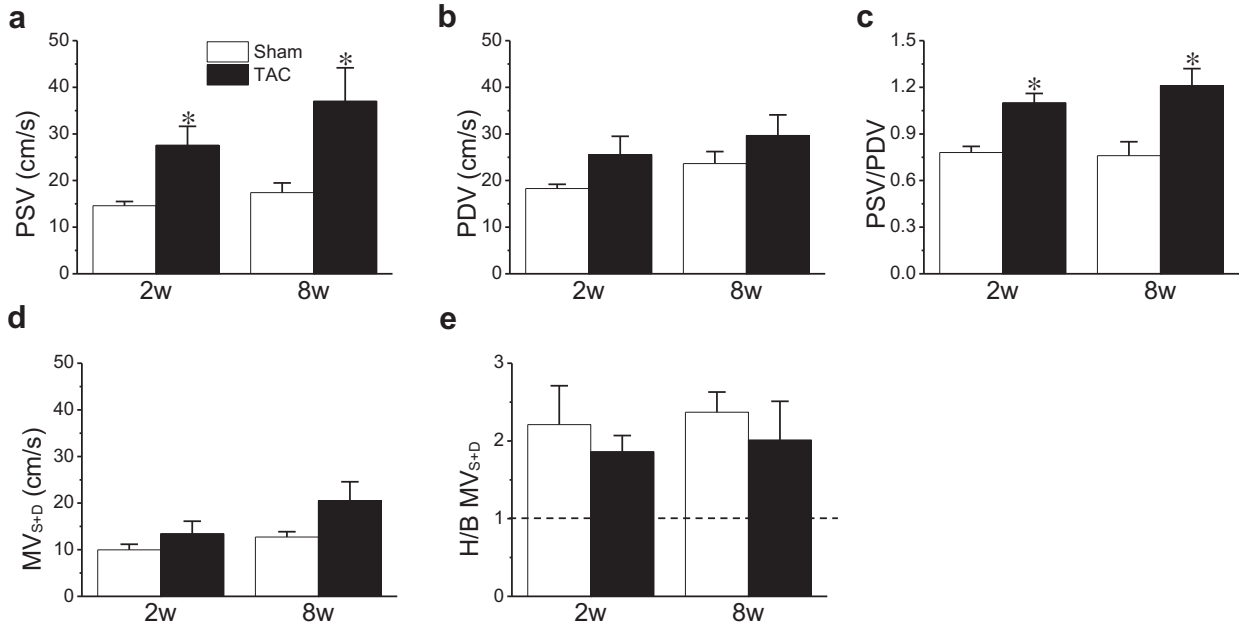

Fig. 4. Baseline Doppler flow parameters (a–d) and coronary flow reserve (CFR) (e) measured from right coronary artery (RCA), with comparison between sham-operated mice and those with transverse aortic constriction (TAC) 2 and 8 wk post-surgery. PSV = peak velocity of systolic wave, PDV = peak velocity of diastolic wave, MV_{S+D} = mean velocity of both the systolic and diastolic waves throughout the cardiac cycle, H/B MV_{S+D} = ratio of MV_{S+D} in hyperemia to that at baseline.*$p < 0.05$ versus corresponding value of sham-operated mice.

the vessel and the different systolic compressive forces seen by the left and right ventricles. In mice, during systole, the left ventricular myocardium compresses the coronary microcirculation to a significant degree, opposing the forward driving force from the aortic pressure and resulting in a low antegrade flow waveform. During diastole, the decompression of coronary microcirculation resulting from the relaxation of myocardium reduces the vascular resistance, leading to a large antegrade flow waveform.

Although the SCA in mice most frequently originates from the RCA and the right coronary sinus (Fernandez et al. 2008; Icardo and Colvee 2001), its phasic flow pattern is similar to that of the LCA, because the septum is anatomically and functionally part of the left ventricle, with a wall thickness similar to that of the left ventricular lateral wall. On the other hand, the SCA had relatively lower flow velocity compared with the LCA, maybe because of the relatively smaller ventricular region that the SCA irrigates.

Compared with the LCA and SCA, the RCA has slightly higher systolic velocity, but much lower diastolic velocity. Right ventricular wall thickness is less than 50% that of the left ventricle, and thus, the right ventricular myocardium produces less compression on the coronary microcirculation during systole and less decompression during the diastole. The peak E/A ratio of tricuspid inflow, which is less than 1 in the present study and our previous studies (Zhou et al. 2003, 2005), also suggests that the right ventricular myocardial active relaxation during diastole is weak in mice. On the other hand, the right ventricle has much lower myocardial mass than the left ventricle (the ratio of right ventricle to left ventricle and septum is 0.24) (Tabima et al. 2010), accounting for the generally lower flow velocity of the RCA.

Effect of TAC on the flow pattern of three coronary arteries

Remodeling of the coronary arterial system is involved in left ventricular hypertrophy because of the pressure overload caused by aortic stenosis and hypertension in humans (Neishi et al. 2005; Nemes et al. 2009; Spaan et al. 2008). With the progress of the diseases, the hypertrophic left ventricle, with compromised function at the beginning, will eventually develop a decompensated condition with congestive heart failure (Lygate et al. 2007). It is thought that heart failure ensues only after the CFR is exhausted (Hartley et al. 2008). Therefore, the coronary arterial perfusion has been intensively studied and the CFR is commonly measured from the LCA using Doppler echocardiography (Gan et al. 2004; Graziosi et al. 2007; Hartley et al. 2008; Meimoun and Tribouilloy 2008; Wikström et al. 2005).

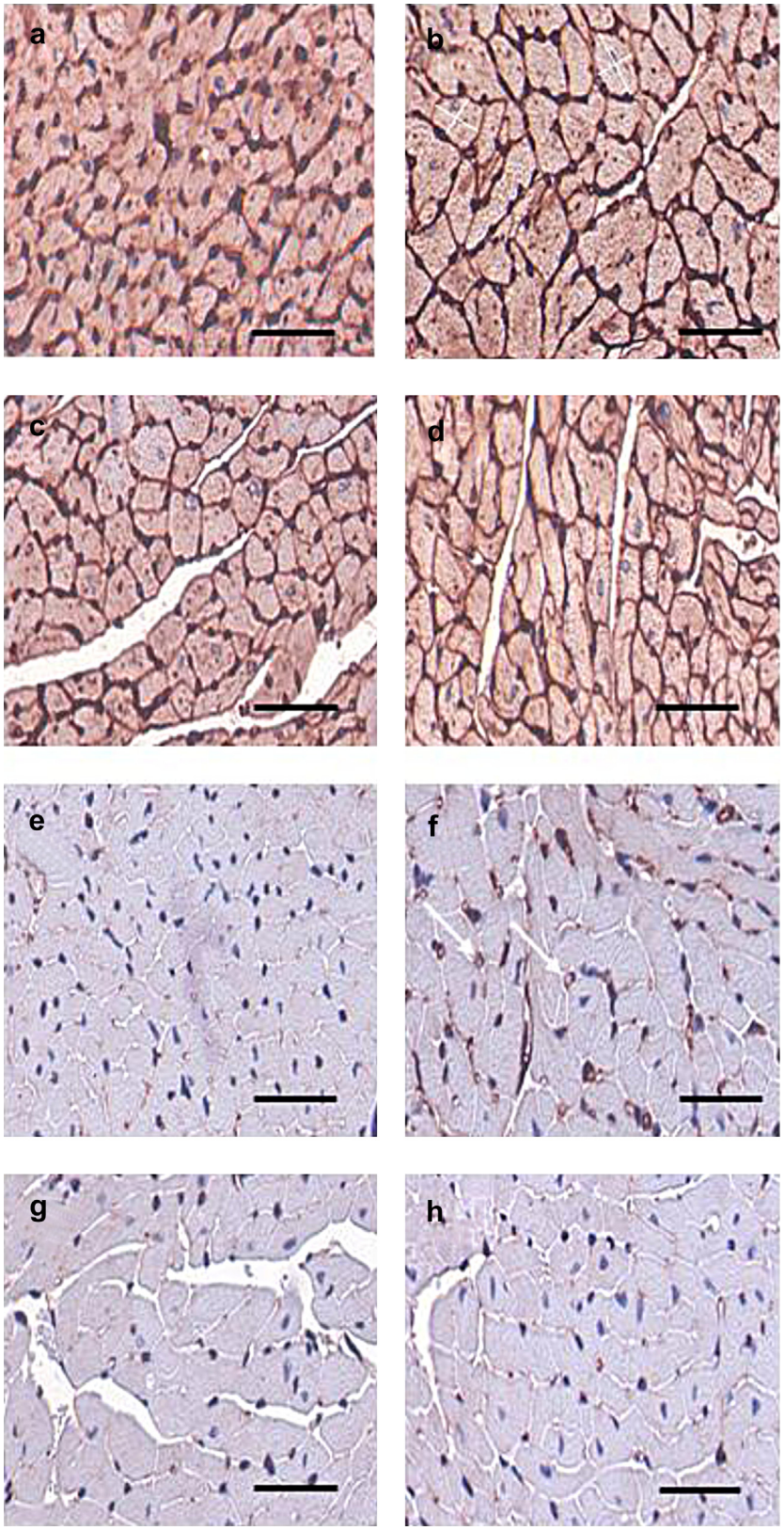

Fig. 5. Representative histologic images of sham-operated mice and mice with transverse aortic constriction (TAC) 2 wk post-surgery. (a, b) Myocytes in left ventricular (LV) lateral wall of sham-operated mice and their counterparts with TAC, respectively. *White bars* indicate the measurement of diameter. (c, d) Myocytes in right ventricular (RV) free wall of

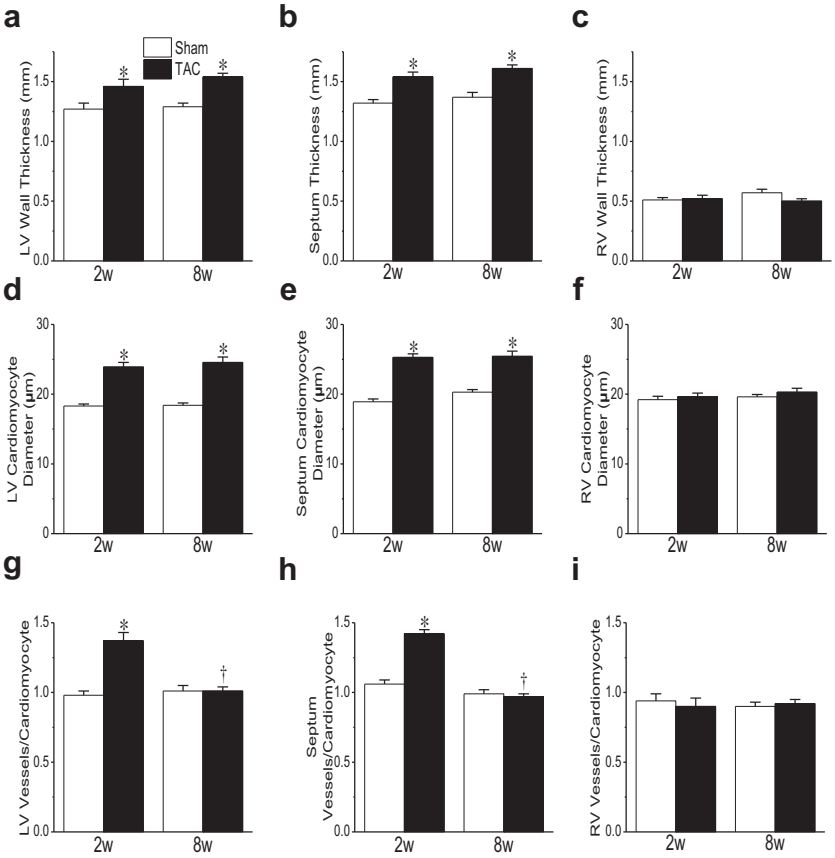

Fig. 6. Comparison of ventricular wall thickness, myocyte size and capillary density between sham-operated mice and mice with transverse aortic constriction (TAC) 2 and 8 wk after surgery. (a–c) Wall thicknesses of left ventricular (LV) lateral wall, septum and right ventricular (RV) free wall, respectively. (d–f) Diameters of myocytes in LV lateral wall, septum and RV free wall, respectively. (g–i) Ratios of capillaries relative to myocytes in the LV lateral wall, septum and RV free wall, respectively. $^{*}p < 0.05$ versus corresponding value of sham-operated mice; $^{\dagger}p < 0.05$ versus value of corresponding group 2 wk post-surgery.

On the other hand, a recent study reported a difference in microcirculatory wave patterns between the left and right coronary arteries in relation to the anatomy of left and right ventricles in humans (Hadjiloizou et al. 2008).

In this study, TAC resulted in significant increases in flow velocity in the LCA and SCA. The enhanced coronary perfusion for the left ventricle is believed to meet the increased blood demand of hypertrophic myocardium, and should be most effective and efficient during diastole with the myocardium relaxed and capillary decompressed. The increase in systolic flow velocity is attributable to the elevated aortic systolic pressure, and also suggests a re-distribution of the blood perfusion from the left ventricular endocardium to epicardium (Hartley et al. 2008). This re-distribution of blood perfusion may be further exaggerated by the vasodilator in this study, and may be responsible for the difference in CFRs calculated with and without inclusion of the systolic flow component.

The left ventricular lateral wall and the septum exhibited similar structural remodeling under TAC, with their wall thickness and myocyte size increased at both time points. However, left ventricular systolic function was in a transitional stage to heart failure 8 wk post-TAC, when the overall mean velocity of both the LCA and SCA remained significantly elevated. Pressure overload initially promotes myocardial angiogenesis, which is crucially involved in adaptive ventricular hypertrophy.

sham-operated mice and their counterparts with TAC, respectively. (e, f) Capillaries in LV lateral wall of sham-operated mice and their counterparts with TAC, respectively. *White arrows* indicate capillaries. (g, h) Capillaries in RV free wall of sham-operated mice and their counterparts with TAC, respectively. Black scale bar = 50 μm.

However, the sustained pressure overload impairs angiogenesis and makes systolic function convert from compensatory status to heart failure (Sano et al. 2007). We postulate that the partially preserved CFR for the left ventricle 2 wk post-TAC might be attributable to the significant neo-angiogenesis, which increases the vascular capacity and reserve of the coronary circulation. The reduced neo-agniogenesis 8 wk post-TAC might be the major mechanism for the decrease in CFR and the ensuing left ventricular systolic dysfunction, implicating the predictive role of CFR measurement.

The left ventricular CFR in this study is similar to those of previous publications obtained by ultrasound (Wikström et al. 2005) and magnetic resonance angiography (Cochet et al. 2010, 2013) in wild-type mice. However, compared with another study (Hartley et al. 2008), the present data indicate a slower and less significant decrease in left ventricular CFR post-TAC. A possible reason is that in our study, the hyperemia was induced by adenosine, rather than high-concentration isoflurane (2.5%), which might cause cardiac depression (Ding et al. 2011), especially in mice with heart disease (You et al. 2012), and reduce the driving forces for coronary perfusion and thus minimize CFR measurement. It is also possible that the mice with TAC in our study had a relatively moderate pressure overload because a slightly larger needle (26 gauge) was used to induce constriction.

At both time points, the flow dynamics of the RCA under TAC did not significantly change in terms of overall mean velocity and CFR. Correspondingly, the right ventricle exhibited no significant change, in ventricular wall thickness, myocyte size, myocardial neoangiogenesis or diastolic function.

Limitations

Doppler color flow imaging revealed the dilation of coronary arteries (appearing as wider color stripes) post-TAC, but their diameters were not measured because of the resolution limit of the current system. A transducer of higher frequency (40 MHz) would facilitate the dimensional measurement, at least for the proximal segment of coronary arteries, allowing for precise assessment of flow.

Isoflurane for anesthesia also has a dose-dependent vasodilating property and has even been used for measuring CFR (Hartley et al. 2008). Therefore it might have a synergetic effect and, to some extent, confound the CFR measurement using adenosine. Nevertheless, the concentration of isoflurane was strictly limited to 1.5% for all experiments to minimize possible bias.

The measurement of coronary flow using Doppler may have variations. As reported in our previous study (Wu et al. 2012a), the Doppler coronary flow velocity measurement had very good reproducibility (Intra-observer and inter-observer variability rates were 1.31% and 2.48%, respectively). Therefore, such reproducibility measurements were not repeated in this study.

CONCLUSIONS

This study has, for the first time, established a protocol for quantitatively evaluating flow dynamics in three major coronary arteries in mice using high-frequency ultrasound. The established method and presented baseline data will facilitate in-depth exploration into the mechanisms in mouse models related to coronary arterial diseases. Mouse models, with genetic modification and surgical intervention, will allow for the determination of genetic factors that modulate the remodeling of the heart and coronary vasculature under pressure overload.

Transverse aortic constriction alters coronary flow patterns, but in distinct ways for each of the three coronary arteries. Through comparison of the left and right sides of the heart, the findings so far have clarified that the pressure overload to the ventricle and the elevated perfusion pressure to the coronary artery have clearly different effects on the remodeling of myocardium and the adaptation of coronary vasculature. It would also be of great interest to find out whether pharmacologic enhancement of neo-angiogenesis delays or partially rescues the deterioration of left ventricular systolic function during pressure overload. In that way, the observations from the mouse model would be informative for clinical therapeutics.

Acknowledgments—The authors thank Christine Laliberté, Shoshana Spring, Brige Chugh (Mouse Imaging Centre) and Qiang Xu (The Centre for Modeling Human Disease) for their help. This work is part of the Mouse Imaging Centre at the Hospital for Sick Children and the University of Toronto. The infrastructure was funded by the Canada Foundation for Innovation and Ontario Innovation Trust. The research was funded by a CIHR grant (102590), an Ontario Research and Development Challenge Fund and the Heart and Stroke Foundation of Ontario (HSFO, Grants T6107 and T6060). R.M.H. holds a Canada Research Chair.

REFERENCES

Ahn D, Cheng L, Moon C, Spurgeon H, Lakatta EG, Talan MI. Induction of myocardial infarcts of a predictable size and location by branch pattern probability-assisted coronary ligation in C57 BL/6 mice. Am J Physiol Heart Circ Physiol 2004;286:H1201–H1207.

Bjørnstad JL, Sjaastad I, Nygård SS, Hasic A, Ahmed MS, Attramadal H, Finsen AV, Christensen G, Tønnessen T. Collagen isoform shift during the early phase of reverse left ventricular remodelling after relief of pressure overload. Eur Heart J 2011;32:236–245.

Braun A, Trigatti BL, Post MJ, Sato K, Simons M, Edelberg JM, Rosenberg RD, Schrenzel M, Krieger M. Loss of SR-BI expression leads to the early onset of occlusive atherosclerotic coronary artery disease, spontaneous myocardial infarctions, severe cardiac dysfunction, and premature death in apolipoprotein E-deficient mice. Circ Res 2002;90:270–276.

Ceci M, Gallo P, Santonastasi M, Grimaldi S, Latronico MV, Pitisci A, Missol-Kolka E, Scimia MC, Catalucci D, Hilfiker-Kleiner D, Condorelli G. Cardiac-specific overexpression of E40 K active Akt prevents pressure overload-induced heart failure in mice by

increasing angiogenesis and reducing apoptosis. Cell Death Differ 2007;14:1060–1062.
Cochet H, Lefrancois W, Montaudon M, Laurent F, Pourtau L, Miraux S, Parzy E, Franconi JM, Thiaudiere E. Comprehensive phenotyping of salt-induced hypertensive heart disease in living mice using cardiac magnetic resonance. Eur Radiol 2013;23:332–338.
Cochet H, Montaudon M, Laurent F, Calmettes G, Franconi JM, Miraux S, Thiaudiere E, Parzy E. In vivo MR angiography and velocity measurement in mice coronary arteries at 9.4 T: Assessment of coronary flow velocity reserve. Radiology 2010;254:441–448.
Davies JE, Whinnett ZI, Francis DP, Manisty CH, Aguado-Sierra J, Willson K, Foale RA, Malik IS, Hughes AD, Parker KH, Mayet J. Evidence of a dominant backward-propagating "suction" wave responsible for diastolic coronary filling in humans, attenuated in left ventricular hypertrophy. Circulation 2006;113:1768–1778.
Ding W, Li Z, Shen X, Martin J, King SB, Sivakumaran V, Paolocci N, Gao WD. Reversal of isoflurane-induced depression of myocardial contraction by nitroxyl via myofilament sensitization to Ca^{2+}. J Pharmacol Exp Ther 2011;339:825–831.
Fernandez B, Duran AC, Fernandez MC, Fernandez-Gallego T, Icardo JM, Sans-Coma V. The coronary arteries of the C57 BL/6 mouse strains: Implications for comparison with mutant models. J Anat 2008;212:12–18.
Foster FS, Mehi J, Lukacs M, Hirson D, White C, Chaggares C, Needles A. A new 15–50 MHz array-based micro-ultrasound scanner for preclinical imaging. Ultrasound Med Biol 2009;35: 1700–1708.
Gan LM, Wikstrom J, Bergstrom G, Wandt B. Non-invasive imaging of coronary arteries in living mice using high-resolution echocardiography. Scand Cardiovasc J 2004;38:121–126.
Graziosi P, Ianni B, Ribeiro E, Perin M, Beck L, Meneghetti C, Mady C, Martinez Filho E, Ramires JA. Echocardiographic and hemodynamic determinants of right coronary artery flow reserve and phasic flow pattern in advanced non-ischemic cardiomyopathy. Cardiovasc Ultrasound 2007;5:31.
Hadjiloizou N, Davies JE, Malik IS, Aguado-Sierra J, Willson K, Foale RA, Parker KH, Hughes AD, Francis DP, Mayet J. Differences in cardiac microcirculatory wave patterns between the proximal left mainstem and proximal right coronary artery. Am J Physiol Heart Circ Physiol 2008;295:H1198–H1205.
Hartley CJ, Reddy AK, Madala S, Michael LH, Entman ML, Taffet GE. Doppler estimation of reduced coronary flow reserve in mice with pressure overload cardiac hypertrophy. Ultrasound Med Biol 2008; 34:892–901.
Hartley CJ, Taffet GE, Reddy AK, Entman ML, Michael LH. Noninvasive cardiovascular phenotyping in mice. ILAR J 2002;43(3): 147–158.
Icardo JM, Colvee E. Origin and course of the coronary arteries in normal mice and in iv/iv mice. J Anat 2001;199:473–482.
Ito N, Nitta Y, Ohtani H, Ooshima A, Isoyama S. Remodelling of microvessels by coronary hypertension or cardiac hypertrophy in rats. J Mol Cell Cardiol 1994;26:49–59.
James TN, Burch GE. Blood supply of the human interventricular septum. Circulation 1958;17:391–396.
Li G, Tokuno S, Tähepôld P, Vaage J, Löwbeer C, Valen G. Preconditioning protects the severely atherosclerotic mouse heart. Ann Thorac Surg 2001;71:1296–1303.
Li Y-H, Reddy AK, Taffet GE, Michael LH, Entman ML, Hartley CJ. Doppler evaluation of peripheral vascular adaptations to transverse aortic banding in mice. Ultrasound Med Biol 2003;29:1281–1289.
Lygate CA, Fischer A, Sebag-Montefiore L, Wallis J, ten Hove M, Neubauer S. The creatine kinase energy transport system in the failing mouse heart. J Mol Cell Cardiol 2007;42:1129–1136.
Meimoun P, Tribouilloy C. Non-invasive assessment of coronary flow and coronary flow reserve by transthoracic Doppler echocardiography: A magic tool for the real world. Eur J Echocardiogr 2008; 9:449–457.
Neishi Y, Akasaka T, Tsukiji M, Kume T, Wada N, Watanabe N, Kawamoto T, Kaji S, Yoshida K. Reduced coronary flow reserve in patients with congestive heart failure assessed by transthoracic Doppler echocardiography. J Am Soc Echocardiogr 2005;18:15–19.
Nemes A, Balázs E, Soliman O, Sepp R, Csanády M, Forster T. Long-term prognostic value of coronary flow velocity reserve in patients with hypertrophic cardiomyopathy: 9-Year follow-up results from SZEGED study. Heart and Vessels 2009;24:352–356.
Rockman HA, Ross RS, Harris AN, Knowlton KU, Steinhelper ME, Field LJ, Ross J Jr, Chien KR. Segregation of atrial-specific and inducible expression of an atrial natriuretic factor transgene in an in vivo murine model of cardiac hypertrophy. Proc Natl Acad Sci USA 1991;88:8277–8281.
Sano M, Minamino T, Toko H, Miyauchi H, Orimo M, Qin Y, Akazawa H, Tateno K, Kayama Y, Harada M, Shimizu I, Asahara T, Hamada H, Tomita S, Molkentin JD, Zou Y, Komuro I. p53-induced inhibition of Hif-1 causes cardiac dysfunction during pressure overload. Nature 2007;446:444–448.
Saraste A, Kyto V, Laitinen I, Saraste M, Leppanen P, Yla-Herttuala S, Saukko P, Hartiala J, Knuuti J. Severe coronary artery stenoses and reduced coronary flow velocity reserve in atherosclerotic mouse model: Doppler echocardiography validation study. Atherosclerosis 2008;200:89–94.
Spaan J, Kolyva C, van den Wijngaard J, ter Wee R, van Horssen P, Piek J, Siebes M. Coronary structure and perfusion in health and disease. Philos Trans A Math Phys Eng Sci 2008;366:3137–3153.
Tabima DM, Hacker TA, Chesler NC. Measuring right ventricular function in the normal and hypertensive mouse hearts using admittance-derived pressure-volume loops. Am J Physiol Heart Circ Physiol 2010;299:H2069–H2075.
Tarnavski O, McMullen JR, Schinke M, Nie Q, Kong S, Izumo S. Mouse cardiac surgery: Comprehensive techniques for the generation of mouse models of human diseases and their application for genomic studies. Physiol Genomics 2004;16:349–360.
Tobita K, Liu X, Lo CW. Imaging modalities to assess structural birth defects in mutant mouse models. Birth Defects Res C Embryo Today 2010;90(3):176–184.
Wikström J, Gronros J, Bergstrom G, Gan LM. Functional and morphologic imaging of coronary atherosclerosis in living mice using high-resolution color Doppler echocardiography and ultrasound biomicroscopy. J Am Coll Cardiol 2005;46:720–727.
Wu J, You J, Jiang G, Li L, Guan A, Ye Y, Li D, Gong H, Ge J, Zou Y. Noninvasive estimation of infarct size in a mouse model of myocardial infarction by echocardiographic coronary perfusion. J Ultrasound Med 2012a;31:1111–1121.
Wu J, You J, Li L, Ma H, Jia J, Jiang G, Chen Z, Ye Y, Gong H, Bu L, Ge J, Zou Y. Early estimation of left ventricular systolic pressure and prediction of successful aortic constriction in a mouse model of pressure overload by ultrasound biomicroscopy. Ultrasound Med Biol 2012b;38:1030–1039.
You J, Wu J, Ge J, Zou Y. Comparison between adenosine and isoflurane for assessing the coronary flow reserve in mouse models of left ventricular pressure and volume overload. Am J Physiol Heart Circ Physiol 2012;303:H1199–H1207.
Yutzey KE, Robbins J. Principles of genetic murine models for cardiac disease. Circulation 2007;115:792–799.
Zhou YQ, Foster FS, Nieman BJ, Davidson L, Chen XJ, Henkelman RM. Comprehensive transthoracic cardiac imaging in mice using ultrasound biomicroscopy with anatomical confirmation by magnetic resonance imaging. Physiol Genomics 2004;18: 232–244.
Zhou YQ, Foster FS, Parkes R, Adamson SL. Developmental changes in left and right ventricular diastolic filling patterns in mice. Am J Physiol Heart Circ Physiol 2003;285:H1563–H1575.
Zhou YQ, Zhu Y, Bishop J, Davidson L, Henkelman RM, Bruneau BG, Foster FS. Abnormal cardiac inflow patterns during postnatal development in a mouse model of Holt-Oram syndrome. Am J Physiol Heart Circ Physiol 2005;289:H992–H1001.